Journal of The Electrochemical Society, **158** (5) H491-H495 (2011)
0013-4651/2011/158(5)/H491/5/$28.00 © The Electrochemical Society

Exciton Localization Behaviors of Basal Stacking Faults in *a*-Plane AlGaN Alloys

Huei-Min Huang,[a] Yung-Chi Wu,[a] and Tien-Chang Lu[a,b,z]

[a]*Department of Photonics and Institute of Electro-Optical Engineering, National Chiao Tung University, Hsinchu 30050, Taiwan*
[b]*Institute of Lighting and Energy Photonics, National Chiao Tung University, Guiren Township, Tainan County, 711 Taiwan*

We study the basal plane stacking faults (BSFs) related optical properties in *a*-plane AlGaN alloys with different Al composition ranging from 0 to 0.28. The low-temperature photoluminescence (PL) spectra for AlGaN show two dominant peaks attributed to the emission of near band edge and BSFs-bound excitons, respectively. The PL integrated intensity ratio of the BSFs to NBE is found to correlate to the density of BSFs observed by the transmission electron microscopy. Finally, the exciton localization behaviors of BSFs in *a*-plane AlGaN alloys is observed and discussed in this study.
 [DOI: 10.1149/1.3561422]

Manuscript submitted September 14, 2010; revised manuscript received January 10, 2011. Published March 11, 2011.

Gallium-nitride (GaN)-based alloys have been generally used as the materials for optoelectronic devices due to their wide direct band gap characteristics with emission spectra covering from infrared to ultraviolet bands. However, conventional *c*-plane multiple quantum well (MQW) structure suffers from the quantum confinement Stark effect (QCSE) as a result of the existence of strong polarization.[1,2] The polarization-induced built-in electric fields along *c*-direction result in spatial separation of electron and hole wave functions leading to the degradation of carrier recombination transition rate, the red-shifted peak emission and the reduction of oscillator strength, which significantly limit the performance of light emitters.[3] The growth along non-polar orientations such as [11–20] *a*-plane and [1–100] *m*-plane has been proved as one of the solutions that polarization-induced effects could be diminished or even eliminated.[4–8] The use of non-polar planes for light emitting devices could consequently be expected.

The structural characteristics of *a*-plane GaN-related material have been widely studied, and the structural defect-related emissions have also been confirmed. The dominant emission peaks of *a*-plane GaN layer in low-temperature spectra do not resemble to *c*-plane GaN materials. The defect-related emission and the interband transition emission for *a*-plane GaN layer have been investigated and clarified by performing cathodoluminescence (CL) and transmission electron microscopy (TEM) on the same region.[9] The emission peak at 3.42 eV in *a*-plane GaN, attributed to excitons bound to basal plane stacking faults (BSFs), has been detailed discussed by temperature, intensity and polarization dependences of spectra.[10,11] Though the defect-related properties of *a*-plane GaN have been established, properties of other *a*-plane GaN-based material systems such as AlGaN and InGaN are not well studied. In particular, AlGaN alloys have attracted much attention due to their applications in ultraviolet (UV) and deep UV optoelectronic devices.

In this study, the non-polar *a*-plane AlGaN alloys with different Al compositions from 0 to 28% were grown by low-pressure metal-organic chemical vapor deposition (MOCVD) and the room-temperature emission wavelengths from different AlGaN alloys cover the energy range from 3.42 to 3.87 eV with increasing the Al composition. The crystal structure properties of AlGaN alloys have studied by the high-resolution X-ray diffraction (XRD) including θ/2θ scan measurements and reciprocal space mappings (RSM), respectively. The defect-related characteristics of AlGaN layers were examined by TEM. Subsequently, the temperature-dependent photoluminescence (PL) spectra of AlGaN alloys have been analyzed and discussed as well.

[z] E-mail: timtclu@mail.nctu.edu.tw

Experimental

The *a*-plane AlGaN alloys with different Al compositions were grown on $(1\bar{1}02)$ *r*-plane sapphire substrates at 1060 °C by metal organic chemical vapor deposition (MOCVD) reactor. During the growth, trimethylgallium (TMGa), trimethylaluminum (TMAl), and ammonia (NH_3) were the precursors used as sources of Ga, Al, and N in whole epitaxial process, respectively. The *a*-plane AlGaN sample structure consisted of an ultrathin SiN_x layer, a 30-nm-thick AlN nucleation layer (NL), and a 1.8-μm-thick bulk GaN. Finally AlGaN alloys with different Al compositions were grown by changing the molar flux ratio TMAl/(TMAl+TMGa) , and the chamber pressure was set about 1.33×10^4 Pa. The thickness of all AlGaN layers in this study was smaller than 300 nm in order to avoid the formation of surface cracks. After the high resolution x-ray diffraction measurements, we could estimate the Al compositions by the XRD diffraction angle separation between AlGaN and GaN peaks. TEM studies were performed in a Philips Tecnai F-20 (field emission gun) microscope with a 200 kV acceleration voltage. In PL measurements, the excitation source was a frequency tripled Ti:sapphire laser at 266 nm, with the pulse width and repetition rate of 200 fs and 76 MHz, respectively. The luminescence was dispersed by a 0.55 m monochromator with the 2400 grooves/mm grating and detected by a high sensitivity photon multiplier tube (PMT). These samples were mounted in a temperature-tunable cryostat which can reach the temperature as low as 14 K. During the measurements, the excitation power was fixed to be about 5 mW, and the excitation spot size was estimated to be 50 μm in diameter.

Results and Discussion

The Al composition of *a*-plane AlGaN alloys were ranging from 0 to 0.28, which were characterized by high-resolution X-ray diffraction measurement, as shown in Fig. 1. The full-width at half-maximum (fwhm) of x-ray rocking curves (XRC) along the in-plane [0001] *c*-direction and $(1\bar{1}00)$ *m*-direction were also extracted. According to the experimental results, the anisotropy in XRC fwhm values for *a*-plane AlGaN alloys with increasing Al composition were observed and reported elsewhere**,** indicating there's a minimum anisotropic strain when the Al composition is about 0.1.[12] The in-plane anisotropy features of *a*-plane GaN and the basal plane stacking fault related anisotropy of XRC fwhm values in *m*-plane GaN have been studied and revealed that the anisotropy features in XRC fwhm are associated with the density and distribution of BSFs, due to the in-plane growth anisotropy for non-polar nitrides.[13,14]

The temperature-dependent PL experiment of *a*-plane GaN was measured at 15 K, which revealed three main emission peaks in the range from 3.30 to 3.50 eV, as shown in Fig. 2a. The energy peak at

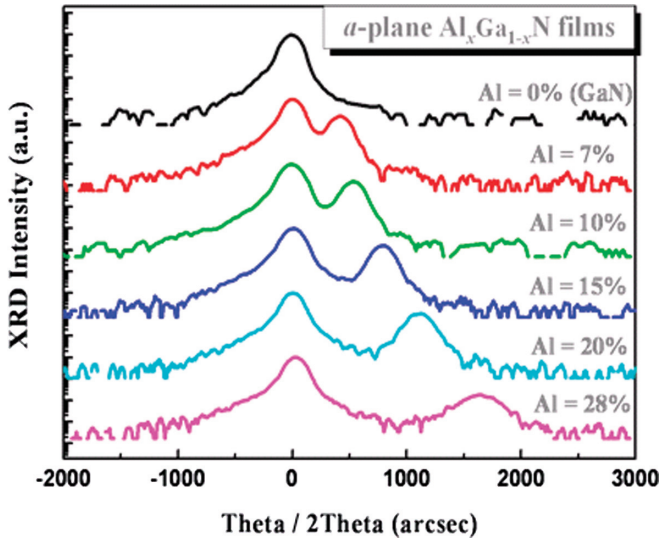

Figure 1. (Color online) High-resolution x-ray diffraction θ/2θ scan for *a*-plane AlGaN alloys.

3.48–3.50 eV is due to the commonly observed GaN near band edge emission (NBE). The NBE consists of two emission peaks assigned to donor-bound exciton (D^0X) and free-exciton (FX) recombination, respectively. However, the D^0X and FX peaks couldn't be clearly specified due to the large inhomogeneous broadening of the emission peaks (~25 meV).[10] One emission band on the right-hand side of NBE at low-temperature can be observed to lie at 3.55 eV. We considered that this shoulder could be the contribution of the free-electron recombination band (FERB). The existence of FERB was related to local unintentional doping nonuniformities and interface sublayers, and usually superimposed over the strong excitonic peak characteristic of the higher quality parts of the film.[15] Furthermore, Paskov et al. indicated that the FERB associated with the triangular-shaped surface defects of *a*-plane GaN in CL measurements.[11]

The emission peak at 3.42 eV arises from the recombination of BSFs-bound excitons, and mainly dominates the low-temperature PL spectra. The BSF, one of the typical of defects in GaN-based materials, could be regarded as a thin layer of a zinc-blende (ZB) material embedded in the wurtzite (WZ) matrix. Excitons are confined in BSF and their recombination energy is 3.42 eV. Nevertheless, the electron wave function of the exciton is confined in the ZB well while the hole wave function is mainly repelled in the wurtzite barriers.[16] The 3.30 eV emission peak was attributed to the partial dislocations terminating the basal plane faults.[9] Paskov et al. also obtained the similar results, and further analyzed the emission at around 3.30 eV associated with DAP-like transition between the impurities decorating the partial dislocation at the BSFs.[10] The free exciton emission dominates the PL spectrum at room temperature due to the thermal quenching of defect-related emissions. According to the peak energy curves shown in Fig. 2b, the emission peaks for NBE transition have an apparent redshift with the increase of temperature. Only the BSFs-bound emission peak follows the so-called s-shaped temperature-dependent behavior, which reflects the lower energy band tail of localized exciton states. The temperature dependence of the NBE emission peak positions of *a*-plane GaN can be well fitted by the empirical Varshni's formula $E_{\text{peak}}(T) = E_g(0) - [\alpha T^2/(T+\beta)]$, as shown in Fig. 2b. We have achieved the best fit for the $E_g(0) \cong 3.49$ eV, $\alpha = 0.8$ meV/K, and $\beta = 1000$ K, which are within the range of those reported for the *a*-plane GaN.[10,17] On the other hand, in order to clarify the s-shaped curve of the BSFs-bound emission peak, we used the modified Varshni's formula to describe such behavior. Hence, the dependence of the emission peak broadening on Al composition x, $\sigma_E(x)$, is combined with the typical Varshni's formula,[18,19] which can be written as

$$E_{\text{peak}}(T) = E_g(T) - \frac{\sigma_E^2}{k_B T} = E_g(0) - \frac{\alpha T^2}{\beta + T} - \frac{\sigma_E^2}{k_B T} \qquad [1]$$

Particularly, σ_E is the standard deviation of exciton emission in the alloy, and it could reflect the magnitude of the potential fluctuations, which is also termed as localization energy. The experimental data for the BSFs curve in Fig. 2b was fitted by the Eq. 1 and the value of σ_E in *a*-plane GaN film was estimated to be about 12 meV at the low temperature. The energy localization effect of BSFs-bound exciton is apt to be easily affected by randomly distributed extrinsic donors in the vicinity of BSFs.[17]

Then, we turn to see the structural and optical properties of *a*-plane AlGaN alloys. Figure 3 show the low-temperature PL spectra of AlGaN alloys with different Al composition. The low-temperature PL spectrum of the AlGaN with Al composition of 0.07 at 15 K was shown in Fig. 3a. The emission peaks below 3.55 eV are related to *a*-

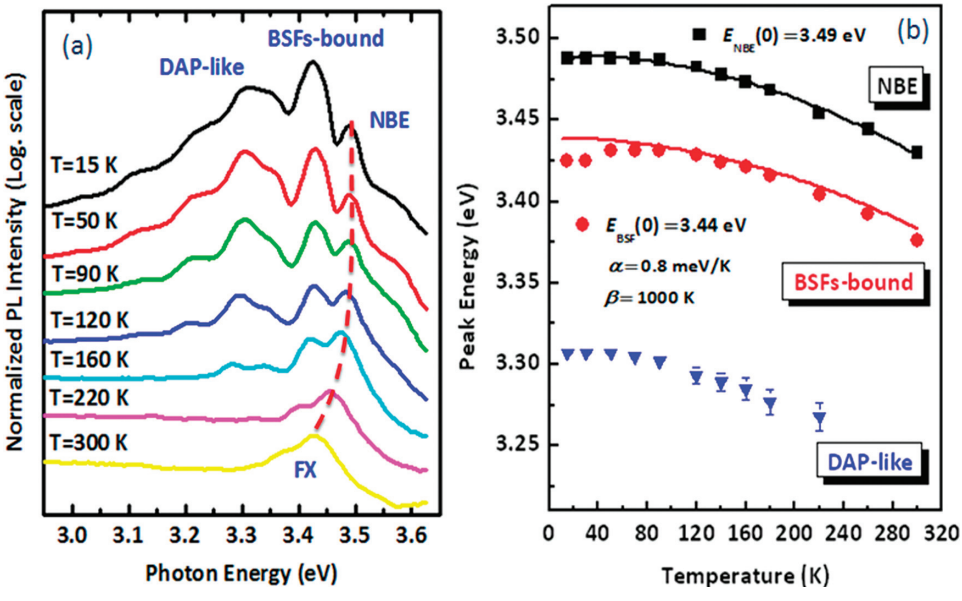

Figure 2. (Color online) Temperature-dependent photoluminescence spectra of *a*-plane GaN are shown in (a) and peak energy positions of NBE, BSFs-bound and DAP-like emissions are summarized in (b).

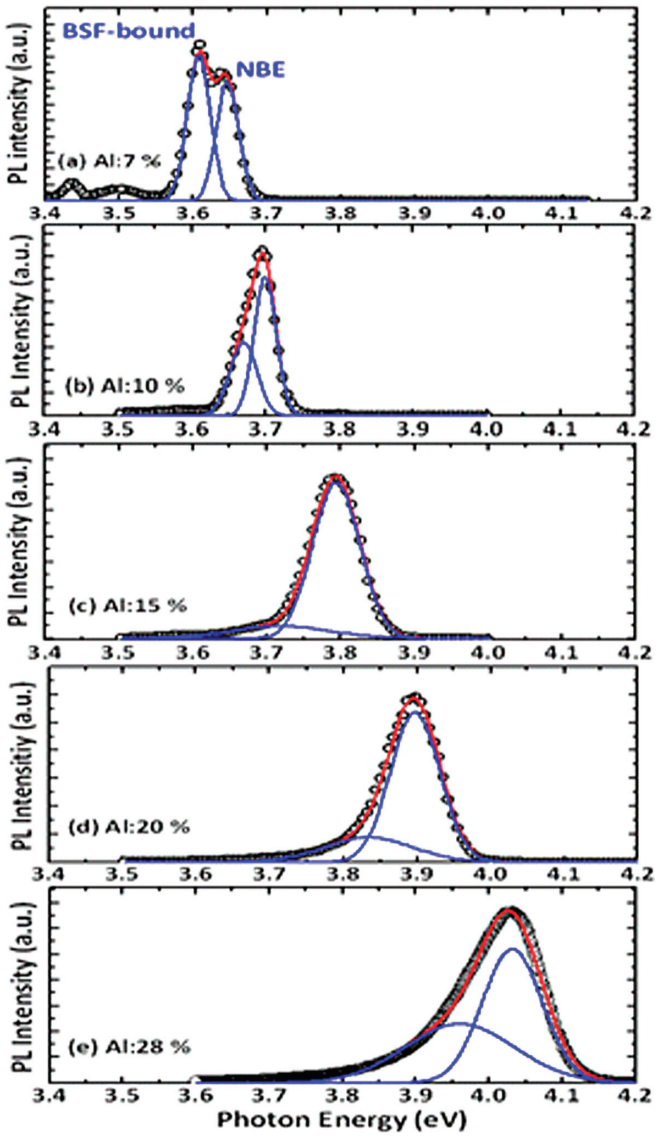

Figure 3. (Color online) Low-temperature PL spectra of AlGaN alloys with different Al composition are fitted based on two Gaussian-type distribution functions, illustrating the influence of BSFs-bound emission and NBE emission, respectively. The open circles are experimental data, the solid lines are the fitted results, and the dashed lines are the contributions of BSFs-bound emission and NBE emission.

plane GaN optical transitions. Aside from these weak peaks, there were two main optical transitions, 3.65, and 3.61 eV emission peaks in the PL spectrum, which are attributed to the AlGaN-related optical

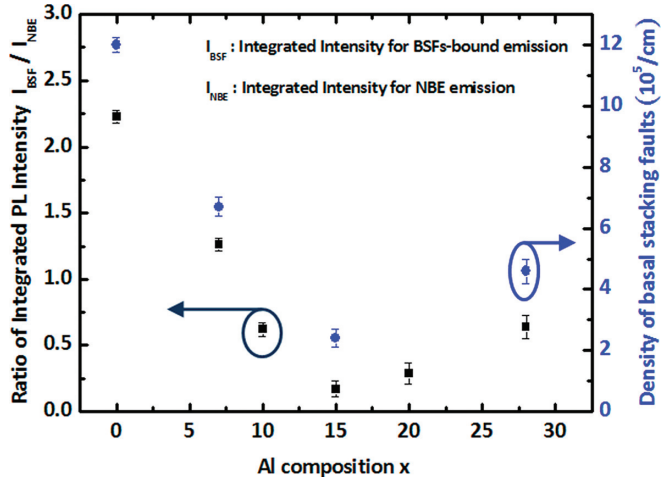

Figure 5. (Color online) The relationship between the PL intensity of BSFs-bound/NBE (left-axis) and the estimated density of BSFs (right-axis) as the Al composition of AlGaN alloys.

transition. The emission of 3.65 eV arises from the NBE emission of $Al_{0.07}Ga_{0.93}N$. The emission of 3.61 eV could be due to the BSFs-bound excitons similar to those in the *a*-plane GaN.[20] Furthermore, the PL spectra of AlGaN alloys could be fitted with two Gaussian-type distribution peaks as shown in Fig. 3, illustrating the influence of BSFs-bound emission and NBE emission, respectively. In general, the fwhm of two Gaussian peaks are larger when increasing the Al composition, indicating the serious infuence of alloy fluctuations in high Al-contained *a*-plane AlGaN alloys. In addition, the ratio of BSFs-bound to NBE peak intensity is denoted as I_{BSF}/I_{NBE}, where $\mathbf{I_{BSF}}$ and $\mathbf{I_{NBE}}$ are the PL integrated intensity for the BSFs-bound and NBE emission respectively, estimated to be 2.33–0.64 with increasing the Al composition. We used the PL integrated intensity ratio to indicate the PL intensity distribution of the BSFs-bound and NBE emission. The relatively lower ratio was observed while Al composition is 0.15. The variation in I_{BSF}/I_{NBE} ratio could be related to the density of BSFs, which can be clarified by the observation of plan-view electron micrograph.

Figure 4 are the bright-field plan-view TEM images taken along the $[11\bar{2}0]$ zone axis showing the distribution of BSFs in *a*-plane AlGaN alloys. As we know, the most dominant defects in *a*-plane AlGaN alloys are basal plane stacking faults, and most of the BSFs are terminated by partial dislocation. The BSFs in *a*-plane WZ nitrides have been identified to be I_1 type.[20] The lowest density of BSFs of 2.4×10^5 cm^{-1} can be observed in the $Al_{0.15}Ga_{0.85}N$ film, which shows the lowest I_{BSF}/I_{NBE} ratio estimated in Fig. 3c. Surprisingly, the observed density of BSFs for these AlGaN alloys have a good agreement with the ratio of I_{BSF}/I_{NBE}. Figure 5 summarized the relationship between the I_{BSF}/I_{NBE} and density of BSFs for different Al compositions. It distinctly indicated that the ratio of

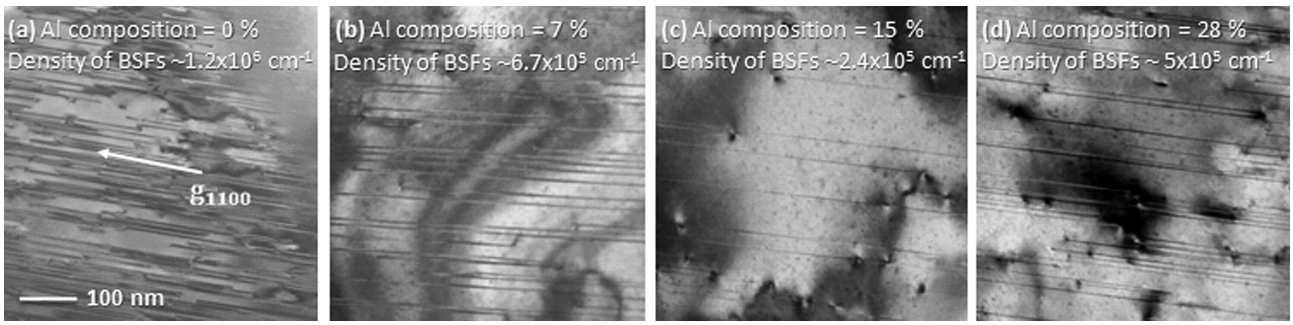

Figure 4. Plane-view TEM images taken under g = $\bar{1}100$ diffraction condition for AlGaN alloys showing the BSFs domains.

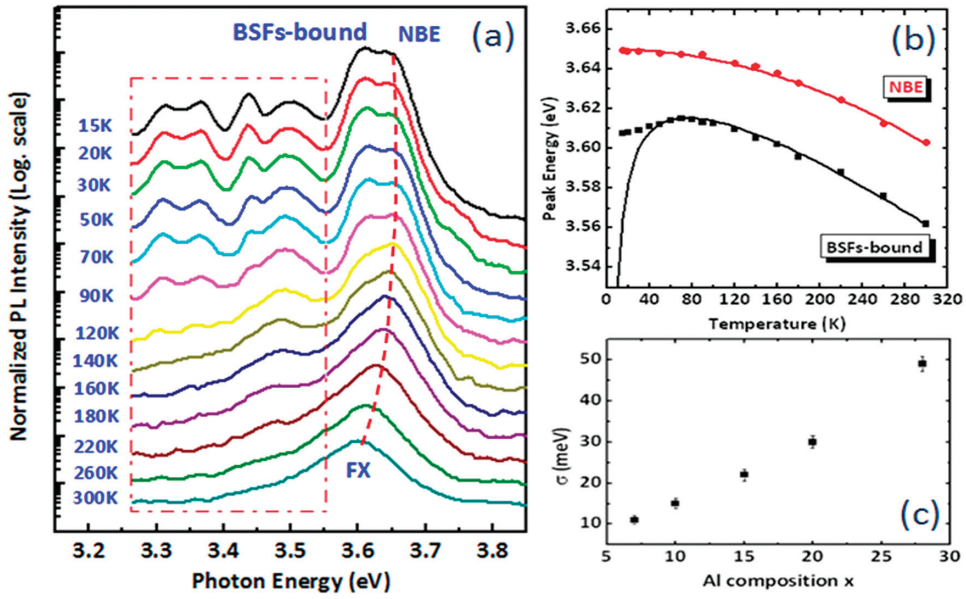

Figure 6. (Color online) (a) PL spectra of *a*-plane AlGaN with an Al composition of 0.07 measured at different temperatures. The part of red-dashed-line below the 3.55 eV is about the emission peak of *a*-plane GaN template. (b) Temperature dependence of the peak energy positions of NBE and BSFs-bound emissions. The solid line curves are fitted with modified Varshni formula. (c) Localization energy σ obtained from the s-shape PL peak position curves for BSFs-bound emission is plotted as a function of Al composition.

I_{BSF}/I_{NBE} depends on the density of BSFs and the optical transition of BSFs in these AlGaN alloys have been identified. The reason that the lowest density of BSFs observed in the $Al_{0.15}Ga_{0.85}N$ film could be due to the smaller anisotropic strain.[12]

The BSFs-related optical properties of *a*-plane AlGaN alloys with different Al compositions were further studied by the temperature-dependent PL spectra. The temperature-dependent PL measurements of *a*-plane AlGaN alloys were performed at temperatures ranging from 15 to 300 K under identical measurement conditions. For example, Fig. 6a shows the temperature-dependent PL measurement result of $Al_{0.07}Ga_{0.93}N$ layer. The BSFs-bound emission peak decreases fast with increasing the temperature, and the shift in emission peak of BSFs-bound appears in PL spectra. At room temperature, the FX emission of about 3.6 eV dominates the PL spectrum due to the thermal quenching of BSFs-bound optical transition. Figure 6b summarized the main emission peaks of $Al_{0.07}Ga_{0.93}N$ layer versus the temperature. The NBE emission peak shifts from about 3.65 to 3.60 eV. The BSFs-bound emission peak shifts toward the higher energy at temperature below 70 K, and then the redshift of emission peak appears above 70 K. As discussed earlier, the s-shaped behavior reflects the localized exciton states. These experimental data were fitted by the Eq. 1, and the value of σ_E was estimated and the relation of σ_E versus the different Al composition was shown in Fig. 6c. The value of σ_E increased from 12 to 49 meV while Al composition increased from 7 to 28%. The nearly linear relationship between the Al composition x and the value of σ_E was observed. The increase of value of σ_E indicates that the degree of the BSFs-related localization increases with increasing the Al composition. There are some possible reasons to account for the increase localization energy. One is due to the alloy fluctuation as observed in Fig. 3 with the increased fwhm in PL spectra when increasing the Al composition. The other is that the randomly distributed extrinsic donors around the basal plane stacking faults are generally regarded as an important explanation for BSFs-related localization effect of *a*-plane GaN.[17] Corfdir et al. further propose that the presence of donor nuclei in the vicinity of the I_1-BSFs in *a*-plane GaN lead to the localization of electrons along the plane of the BSFs.[21] Therefore, we suppose that the increase of σ_E could be attributed to the increase of alloy fluctuation and the growth-induced donors around the BSFs while Al molar flux increased during the growth of *a*-plane AlGaN alloys. In addition, since the electron effective masses of AlGaN alloys were interpolated between $m_{e,\,GaN} = 0.18m_0$ and $m_{e,\,AlN} = 0.27m_0$,[22] and those will increase while the Al compositon increases; it would imply that the larger effective mass could as well cause the increase of value of σ_E.[23–25]

Conclusion

In summary, the BSF-related properties of the non-polar *a*-plane AlGaN alloys grown by MOCVD on *r*-plane sapphire with different Al compositions ranging from 0 to 28% were studied. The density of BSFs for these AlGaN alloys have a linear relationship with the PL integrated intensity ratio of I_{BSF}/I_{NBE}, distinctly identifying important optical transition paths in BSFs of *a*-plane AlGaN alloys. In addition, the BSFs-related localization behavior was observed in *a*-plane AlGaN alloys. With increasing the Al compositon, the increase of localiztion of BSF-bound excitons has been observed for *a*-plane AlGaN alloys. The relationship between optical and structural characteristics of *a*-plane AlGaN alloys presented here shall be beneficial to the growth and design UV and deep UV optoelectronic devices.

Acknowledgment

These works were supported by the MOE ATU program and in part by the National Science Council of Republic of China (ROC) in Taiwan under contract nos. NSC-98-3114-M-009-001 and NSC-96-2221-E-009-094-MY3.

National Chiao Tung University assisted in meeting the publication costs of this article.

References

1. W. H. Sun, J. W. Yang, C. Q. Chen, J. P. Zhang, M. E. Gaevski, E. Kuokstis, V. Adivarahan, H. M. Wang, Z. Gong, M. Su, et al., *Appl. Phys. Lett.*, **83**, 2599 (2003).
2. B. A. Haskell, F. Wu, M. D. Craven, S. Matsuda, P. T. Fini, T. Fujii, K. Fujito, S. P. DenBaars, J. S. Speck, and S. Nakamura, *Appl. Phys. Lett.*, **83**, 644 (2003).
3. F. Bernardini, V. Fiorentini, and D. Vanderbilt, *Phys. Rev. B*, **56**, 10024 (1997).
4. T. S. Ko, T. C. Wang, R. C. Gao, H. G. Chen, G. S. Huang, T. C. Lu, H. C. Kuo, and S. C. Wang, *J. Cryst. Growth*, **300**, 308 (2007).
5. X. Ni, Y. Fu, Y. T. Moon, N. Biyikli, and H. Morkoc, *J. Cryst. Growth*, **290**, 166 (2006).
6. P. Waltereit, O. Brandt, M. Ramsteiner, R. Uecker, P. Reiche, and K. H. Ploog, *J. Cryst. Growth*, **218**, 143 (2000).
7. C. Rivera, J. L. Pau, E. Muñoz, P. Misra, O. Brandt, H. T. Grahn, and K. H. Ploog, *Appl. Phys. Lett.*, **88**, 213507 (2006).
8. P. Waltereit, O. Brandt, A. Trampert, H. T. Grahn, J. Menniger, M. Ramsteiner, M. Reiche, and K. H. Ploog, *Nature (London)*, **406**, 865 (2000).
9. R. Liu, A. Bell, F. A. Ponce, C.Q. Chen, J. W. Yang, and M. A. Khan, *Appl. Phys. Lett.*, **86**, 021908 (2005).
10. P. P. Paskov, R. Schifano, B. Monemar, T. Paskova, S. Figge, and D. Hommel, *J. Appl. Phys.*, **98**, 093519 (2005).
11. P. P. Paskov, T. Paskova, B. Monemar, S. Figge, D. Hommel, B. A. Haskell, P. T. Fini, J.S. Speck, and S. Nakamura, *Superlattices Microstruct.*, **40**, 253 (2006).
12. H. M. Huang, S. C. Ling, J. R. Chen, T. S. Ko, J. C. Li, T. C. Lu, H. C. Kuo, and S. C. Wang, *J. Cryst. Growth*, **312**, 869 (2010).

13. T. Zhu, D. Martin, R. Butte, J. Napierala, and N. Grandjean, *J. Cryst. Growth*, **300**, 186 (2007).
14. M. B. McLaurin, A. Hirai, E. Young, F. Wu, and J. S. Speak, *Jpn. J. Appl. Phys.*, **47**, 5429 (2008).
15. B. Arnaudov, T. Paskova, E. M. Goldys, S. Evtimova, and B. Monemar, *Phys. Rev. B*,**64**, 045213 (2001).
16. C. Stampfl and C. G. Van de Walle, *Phys. Rev. B*, **57**, R15052 (1998).
17. P. Corfdir, P. Lefebvre, J. Levrat, A. Dussaigne, J. D. Ganière, D. Martin, J. Ristić, T. Zhu, N. Grandjean, and B. D. Plédran, *J. Appl. Phys.*, **105**, 043102 (2009).
18. A. Bell, S. Srinivasan, C. Plumlee, H. Omiya, F. A. Ponce, J. Christen, S. Tanaka, A. Fujioka, and Y. Nakagawa, *J. Appl. Phys.*, **95**, 4670 (2004).
19. P. G. Eliseev, P. Perlin, J. Lee, and M. Osinski, *Appl. Phys. Lett*. **71**, 569 (1997).
20. P. Corfdir, P. Lefebvre, L. Balet, S. Sonderegger, A. Dussaigne, T. Zhu, D. Martin, J.-D. Ganière, N. Grandjean, and B. Deveaud-Plédran, *J. Appl. Phys.*, **107**, 043524 (2010).
21. P. Corfdir, P. Lefebvre, J. Ristić, J. D. Ganière, and B. Deveaud-Plédran, *Phys. Rev. B*, **80**, 153309 (2009).
22. M. Suzuki, T. Uenoyama, and A. Yanase, *Phys. Rev. B*,**52**, 8132 (1995).
23. B. K. Meyer, G. Steude, A. Goldner, A. Hoffmann, H. Amano, and I. Akasaki, *Phys. Status Solidi B,* **216**, 187 (1999).
24. N. Nepal, J. Li, M. L. Nakarmi, J. Y. Lin, and H. X. Jiang, *Appl. Phys. Lett.*, **88**, 062103 (2006).
25. H. Murotani, Y. Yamada, T. Taguchi, A. Ishibashi, Y. Kawaguchi, and T. Yokogawa, *J. Appl. Phys.*, **104**, 053514 (2008).